

## $\pi$ conjugation in the epitaxial Si(111)-( $\sqrt{3} \times \sqrt{3}$ ) surface: Unconventional “bamboo hat” bonding geometry for Si

Wei Jiang,<sup>1</sup> Zheng Liu,<sup>2</sup> Miao Zhou,<sup>3</sup> Xiaojuan Ni,<sup>1</sup> and Feng Liu<sup>1,4,\*</sup>

<sup>1</sup>Department of Materials Science and Engineering, University of Utah, Salt Lake City, Utah 84112, USA

<sup>2</sup>Institute for Advanced Study, Tsinghua University, Beijing 100084, China

<sup>3</sup>Department of Physics, Beihang University, Beijing 100191, China

<sup>4</sup>Collaborative Innovation Center of Quantum Matter, Beijing 100084, China

(Received 2 December 2016; published 12 June 2017)

The recently observed ( $\sqrt{3} \times \sqrt{3}$ ) surface reconstruction in heteroepitaxial Si(111) thin films on metal substrates is widely considered as a promising platform to realize two-dimensional Dirac and topological states, yet its formation mechanism and structural stability remain poorly understood, leading to the controversial terminology of “multilayer silicene.” Based on valence bond and conjugation theory, we propose a  $\pi$ -conjugation plus charge-transfer model to elucidate such a unique “bamboo hat” surface geometry. The formation of planar ring-shaped  $\pi$  conjugation and charge transfer from the rings to the upper buckled Si atoms greatly lowers the surface dangling-bond energy. We justify this unconventional Si structural model by analyzing from first-principles surface stress tensors and surface energies as a function of strain. Within the same formalism, additional metastable surface reconstructions with similar “bamboo hat” features are predicted, which opens possibilities to other exotic electronic states in Si.

DOI: 10.1103/PhysRevB.95.241405

$\pi$  conjugation has long been known to play a key role in stabilizing carbon-based planar structures, such as benzene, graphite, and graphene [1–5]. The other group IV elements, however, have a much weaker tendency to form  $\pi$  conjugation, because of their larger atomic radius. For example, all Si allotropes adopt a “three-dimensional (3D)” bonding configuration with fully saturated covalent  $sp^3$  bonds. Weak  $\pi$  conjugation has been found in a Si(111)-(2×1) surface within a linear chain structure [6–8], but the most typical hexagonal ring structure has not been seen. This underlies the difficulty in experimentally synthesizing the elusive freestanding form of silicene [9–14].

Interestingly, a “planar” hexagonal ring-shaped structure has been observed in the surface of epitaxially grown Si(111)-( $\sqrt{3} \times \sqrt{3}$ ) thin films [15–21], which has been dubbed “multilayer silicene” by some researchers. However, previous first-principles calculations have invalidated a stacked silicene structure, which spontaneously transforms into a bulk  $sp^3$  structure with just two layers of stacking [19,20]. Thus, silicene-like electronic properties, such as Dirac cones, should only be attributed to the unique ( $\sqrt{3} \times \sqrt{3}$ ) surface reconstruction. Understanding its formation mechanism will help resolve the longstanding “silicene” puzzle, shedding light on understanding the difficulties of growing freestanding silicene.

On the other hand, the surface properties of Si have been extensively studied for many decades, because of its extraordinary importance to electronic devices [22–29]. The basic surface reconstruction of Si was considered to be well understood, such as (7×7) reconstruction for the annealed and (2×1) reconstruction for the cleaved Si(111) surface. So the recently observed ( $\sqrt{3} \times \sqrt{3}$ ) surface in heteroepitaxial Si(111) thin films is a big surprise, because it is fundamentally different from previous models, especially considering the unusual planar ring structure that is unexpected for Si. Clarifying the

physical mechanism of such a unique surface reconstruction is thus of particular importance, which may profoundly renew our interest in Si surfaces and open a route to realizing Dirac and topological bands in Si surfaces [30–33], as an interesting alternative to silicene.

In this Rapid Communication, we first revisit the traditional surface reconstructions of Si and then propose a  $\pi$ -conjugation plus charge-transfer model to explain the unexpected stability of a Si(111)-( $\sqrt{3} \times \sqrt{3}$ ) surface reconstruction with a “bamboo hat” bonding geometry. Based on density functional theory (DFT) calculations [34], we further analyze the effect of strain on the surface energies of both ( $\sqrt{3} \times \sqrt{3}$ ) and (2×1) superstructures to evaluate their relative stability to elucidate the experimental results [15–17]. Finally, we investigate the possible configurations of Si(111)-( $\sqrt{21} \times \sqrt{21}$ ) reconstruction as observed in a recent experiment [35], which can also be explained by the  $\pi$ -conjugation and charge-transfer model.

For the (111)-oriented Si film, different from the  $\pi$ -stacking interaction in graphite, Si prefers to form  $sp^3$  hybridized  $\sigma$  bonds, and a crossover between silicene and bulk Si is expected when the Si film is thicker than just two layers [19,20]. The ( $\sqrt{3} \times \sqrt{3}$ ) superstructure therefore represents a different surface reconstruction in the Si(111) surface, differing from (7×7) and (2×1) surface reconstructions of bulk-terminated Si. We note that there is also a monolayer ( $\sqrt{3} \times \sqrt{3}$ ) silicene reported on the Ag and Ir substrates [12,13], which is controlled by substrate-induced strain [36]. Although it does serve as a buffer layer for the subsequent ( $\sqrt{3} \times \sqrt{3}$ ) reconstructed layers [20,21], its formation is clearly different.

In forming a Si surface, dangling bonds are created, e.g., one and two dangling bonds per Si atom in the bulk-terminated Si(111) and Si(100) surfaces, respectively, as shown in Figs. 1(a) and 1(d), which are highly unstable. To lower the high surface energy, the dominant mechanism is to lower the dangling-bond energy through surface reconstructions. In principle, there are two ways to lower the dangling-bond energy [22,37–39]. One is obviously to remove the dangling

\*Corresponding author: fliu@eng.utah.edu

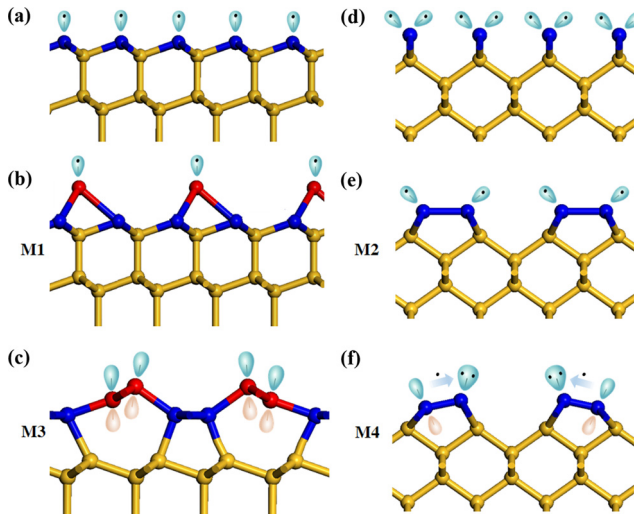


FIG. 1. Schematic view of different mechanisms of Si surface reconstruction. (a) and (d) Bulk-terminated Si(111) and Si(100) surfaces with one and two dangling bonds, respectively. (b) The structure with adatoms (red) that saturate the surface dangling bonds in the Si(111)-(7×7) surface. (c) Formation of  $\pi$ -conjugated chain (red) through couplings between neighboring  $p$  orbitals in the Si(111)-(2×1) surface. (e) The formation of dimers that reduce one dangling bond per surface atom. (f) The buckling induces charge transfer from the down-buckled to up-buckled atom to form empty  $p_z$  and electron lone pairs, respectively, in the Si(100)-(2×1) surface.

bonds, which can be achieved by adsorbing adatoms directly over the surface layer, as shown in Fig. 1(b) (hereafter referred to as mechanism M1) or creating dimers to form a covalent bond between two dangling bonds, as shown in Fig. 1(e) (M2). The other way is to take the advantage of  $\pi$  conjugation (M3) and charge transfer (M4). The  $\pi$  conjugation can be achieved through coupling between neighboring  $p$  orbitals, in either a linear chain or ring shape, in principle. So far, however, only a  $\pi$ -conjugated chain was reported on the Si(111)-(2×1) surface [Fig. 1(c)]. Charge transfer, as manifested in dimer buckling [see Fig. 1(f)], lowers the energy by the Jahn-Teller effect, transferring electrons from the down-buckled to the up-buckled atom to form empty and filled (lone pair) dangling bonds, respectively.

In general, two or more mechanisms cooperate to stabilize a surface reconstruction. For example, in the Si(111) surface, the most stable (7×7) superstructure was explained by the dimer-adatom-stacking-fault model [28], which consists of both M1 and M2, and the metastable (2×1) surface was clarified by a combination of M2 and M3 (Pandey model) [8]. Also, M3 and M4 were used to explain Si(100)-(2×1) reconstruction [29]. Here, we will apply some of these same principles to understand the recently observed Si(111)-( $\sqrt{3} \times \sqrt{3}$ ) surface [15–21].

As shown in Fig. 2(a), among six Si atoms in the optimized ( $\sqrt{3} \times \sqrt{3}$ ) surface, three atoms (light blue) are bonded with the underlying Si (BL-Si), one (red) is highly buckled (HB-Si), and the other two (deep blue) are almost unbuckled (UB-Si). The BL-Si atoms form four bonds with the surface and Si atoms

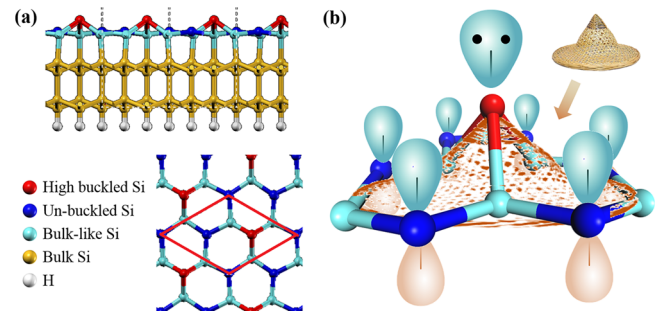


FIG. 2. Analysis of the structural property of the ( $\sqrt{3} \times \sqrt{3}$ ) superstructure in a Si(111) surface. (a) Side and top view of the ( $\sqrt{3} \times \sqrt{3}$ ) surface. The red lines indicate the unit cell. (b) Schematic view of  $\pi$  conjugation and an electron lone pair in the ( $\sqrt{3} \times \sqrt{3}$ ) surface with the inset indicating the bamboo hat geometry.

underneath, showing an  $sp^2 + \sigma$  hybridization. In contrast, the UB-Si and HB-Si atoms have only three bonds with their nearest neighbors (NNs) and form a “planar” structure with a small buckling height around 0.2 Å and a typical tetrahedral structure, respectively [34]. The former indicates an  $sp^2$  hybridized state with an unhybridized  $p_z$  orbital and the latter has an  $sp^3$  hybridized state with a lone pair of electrons. Similar to  $\pi$  conjugation in graphene, to increase the stability, the UB-Si with unhybridized  $p_z$  orbitals, arranged in a hexagonal lattice, form delocalized  $\pi$  bonds through the conjugated  $\pi$ - $\pi$  interaction. On the other hand, the HB-Si is further stabilized via charge transfer from the UB-Si to form a lone pair [Fig. 2(b)].

The overall structure of this peculiar bonding configuration closely resembles a bamboo hat shape (BHS), as shown in Fig. 2(b). In the following, we refer to it as the BHS surface. Note that, different from M4 where charge is transferred directly between two bonded atoms, the charge transfer here occurs indirectly through the bridging BL-Si atoms; also different from M3 where  $\pi$  conjugation is formed by the NNs, the  $\pi$  conjugation here is in between the next NNs. This is an example that has a planar ring-shaped  $\pi$  conjugation in the bulk Si surface. We note a similar structure has been reported in the proposed dumbbell-shaped silicene and germanene structures [40–42].

To further verify this intriguing bonding structure for Si, we calculated the band structure along special  $K$  points and the projected density of states (PDOS) around the Fermi level for the BHS surface. As shown in Figs. 3(a) and 3(b), the nearly flat band (FB) associated with the  $sp^3$  hybridized states for HB-Si atoms lies below the Fermi level (red band) and is fully filled, indicating a lone pair. Similar to graphene, the hexagonal lattice consisting of unhybridized  $p_z$  orbitals of the UB-Si produces a Dirac cone [blue bands in Fig. 3(a)] with a linear dispersive band near the  $K$  point (see the magnified view in Fig. S1 [34]), indicating  $\pi$  conjugation among UB-Si atoms. Different from the half-filled  $\pi$  bands in graphene where the Fermi level is located exactly at the Dirac point, the Dirac bands here are one-fourth filled, which confirms the electron transfer from the UB-Si to the HB-Si atoms. Due to a longer hopping distance, the calculated bandwidth

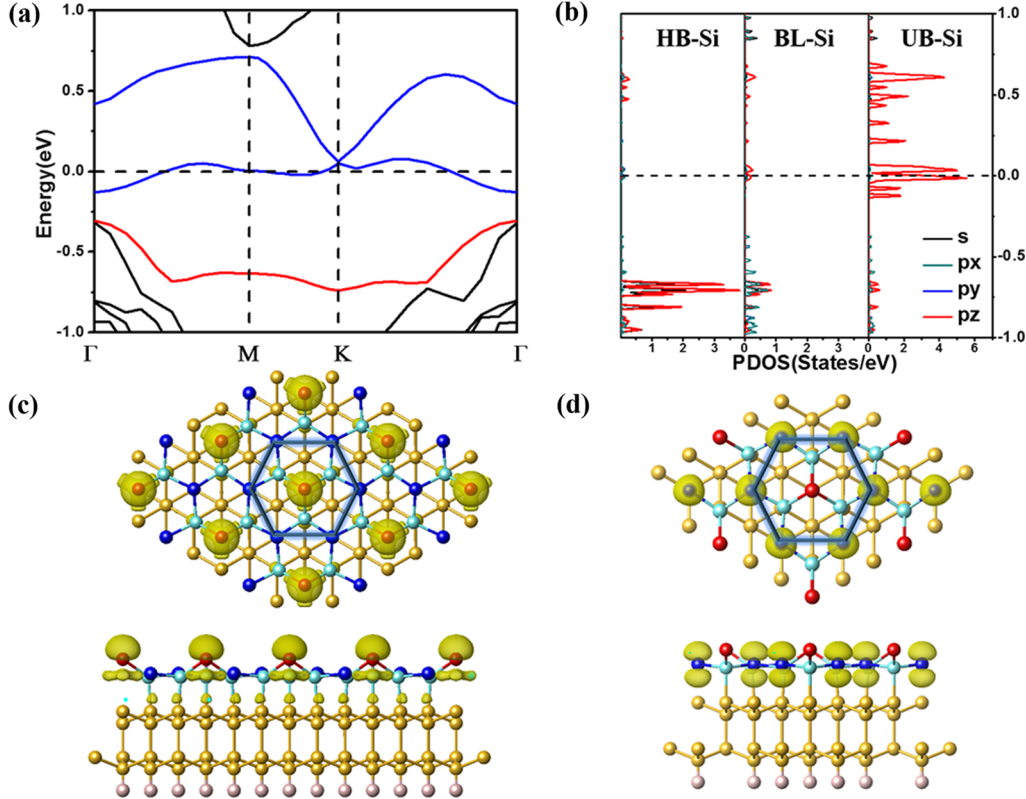


FIG. 3. DFT simulation. (a) and (b) Band structure and the projected density of states of the  $(\sqrt{3} \times \sqrt{3})$  surface reconstruction. The one-fourth filled unhybridized  $p_z$  orbitals of the UB-Si form the Dirac bands (blue bands), while  $sp^3$  hybridized orbitals of HB-Si are fully occupied and lie under the Fermi level (red band). (c) and (d) Top and side views of the partial charge distribution of the FB and the Dirac band displaying a clear  $sp^3$  and  $sp^2$  hybridized orbital shape around HB-Si and UB-Si atoms, respectively. The central blue hexagon highlights the  $\pi$  conjugation.

and the Fermi velocity are relatively smaller than those in graphene. In addition, to confirm the hybridization nature of the surface atoms, we calculated the partial charge densities for the Dirac bands and the FB underneath, respectively, as shown in Figs. 3(c) and 3(d). The charge densities for the FB are mainly localized around the HB-Si atoms, and a clear  $sp^3$  hybridized orbital shape can be seen [Fig. 3(c)]. On the other hand, the Dirac bands are verified to consist of dumbbell-shaped  $p_z$  orbitals from the UB-Si atoms arranged in a hexagonal lattice [blue hexagon in Fig. 3(d)]. To better understand the surface electronic structure, we also calculated a  $(\sqrt{3} \times \sqrt{3})$  monolayer structure model and constructed an effective tight-binding Hamiltonian [34], which confirm that the BHS surface is stabilized by the cooperative effects of the ring-shaped  $\pi$ -conjugation and charge-transfer effect.

It is well known that thin films are grown under conditions far from equilibrium, so that the resulting surface reconstructions are generally metastable. They form via specific kinetic pathways for given growth conditions (e.g., at a low temperature), but remain dynamically stable at given temperatures. This is also the case for the  $(\sqrt{3} \times \sqrt{3})$  surface, which only forms at low temperatures ( $\sim 200^\circ\text{C}$ ) and has a compressed lattice constant [16–18]. Therefore, to better understand its formation, we next analyze the relative stability of the BHS surface and the bulk-terminated  $(2 \times 1)$  surface as a function of strain. We first calculated the surface

energy ( $\gamma$ ), surface stress tensors ( $\sigma$ ), and stress anisotropies ( $F$ ) in the unstrained Si(111) surface using the following equations,

$$\gamma = \frac{1}{2A} (E_{\text{slab}}^N - N \Delta E), \quad (1a)$$

$$\Delta E = \frac{(E_{\text{slab}}^N - E_{\text{slab}}^{N-2})}{2}, \quad (1b)$$

where  $A$  is the surface area,  $E_{\text{slab}}^N$  is the total energy of slabs that contain  $N$  number of atomic layers, and  $\Delta E$  represents the total energy for one layer of bulk Si atoms, as calculated using Eq. (1b). To describe the surface stress tensor, for the  $(2 \times 1)$  superstructure, the  $x$  and  $y$  directions were set perpendicular to and along the  $\pi$ -conjugated chains, respectively, while for the BHS surface, the  $x$  and  $y$  directions were set arbitrarily given its structural isotropy (Fig. S3) [34]. We used positive values to indicate tensile stress, and summarized the calculated results in Table I. The unstrained surface energies for  $(\sqrt{3} \times \sqrt{3})$  and  $(2 \times 1)$  superstructures are 90.5 and 86.8 meV/ $\text{\AA}^2$ , respectively, which are relatively higher than the experimental value for the most stable Si(111) surface (76.8 meV/ $\text{\AA}^2$  [43]). Both systems exhibit a tensile stress with the  $(2 \times 1)$  surface having dramatically higher values than the BHS surface. Moreover, the  $(2 \times 1)$  surface shows a large surface stress anisotropy, caused by the alternating buckled  $\pi$ -bonded chains that tend to shrink the surface in a direction perpendicular to the chain.

TABLE I. Surface energies ( $\gamma$ ), stress tensors ( $\sigma$ ), and stress anisotropies ( $F$ ) of  $(\sqrt{3} \times \sqrt{3})$  and  $(2 \times 1)$  reconstructions in the Si(111) surface calculated using first-principles methods.

No. of layers	$\sqrt{3} \times \sqrt{3}$				$2 \times 1$			
	$\gamma$ (meV/ $\text{\AA}^2$ )	$\sigma_{xx}$ (meV/ $\text{\AA}^2$ )	$\sigma_{yy}$ (meV/ $\text{\AA}^2$ )	$F$ (meV/ $\text{\AA}^2$ )	$\gamma$ (meV/ $\text{\AA}^2$ )	$\sigma_{xx}$ (meV/ $\text{\AA}^2$ )	$\sigma_{yy}$ (meV/ $\text{\AA}^2$ )	$F$ (meV/ $\text{\AA}^2$ )
3	86.7	45.6	45.6	0.0	89.9	268.4	80.5	187.9
4	89.9	53.7	58.0	-4.3	85.5	250.3	81.1	169.2
5	89.9	54.3	54.9	-0.6	86.8	269.0	89.3	179.7
6	90.5	53.7	53.7	0.0	86.8	271.5	89.9	181.6
7	90.5	51.2	53.7	-2.5	86.8	270.3	91.1	179.2
8	89.9	49.3	52.4	-3.1	86.8	269.0	86.8	182.2

Using the above calculation results, we can estimate the relative surface energy under strain using  $\gamma_s(\varepsilon) = \gamma_0 + \sigma \varepsilon$ , where  $\gamma_0$  is the calculated unstrained surface energy,  $\sigma$  is the stress tensor, and  $\varepsilon$  is the strain with a positive value indicating tensile strain. Surface energies as a function of strain are (see also Fig. S4 [34])

$$\gamma_{(\sqrt{3} \times \sqrt{3})}(\varepsilon) = 90.5 + 106.7\varepsilon, \quad (2a)$$

$$\gamma_{(2 \times 1)}(\varepsilon) = 86.8 + 359.5\varepsilon. \quad (2b)$$

We note that the BHS structure is only more stable than the  $(2 \times 1)$  surface when the surface is under a tensile strain larger than 1.5%, otherwise it is less stable [34]. This is consistent with the experimental observations that the  $(\sqrt{3} \times \sqrt{3})$  structure is metastable with a lattice contraction of compressive strain [16–18]. The kinetic pathways leading to the formation of a  $(\sqrt{3} \times \sqrt{3})$  structure deserve further attention. On the other hand, we have carried out molecular dynamic simulations to confirm its dynamic stability upon formation up to 500 K (Fig. S5 [34]).

Finally, we extended our calculation from a  $(\sqrt{3} \times \sqrt{3})$  to a  $(\sqrt{21} \times \sqrt{21})$  superstructure to explore other possible buckled surface geometries that may be observed during the “silicene” growing processes [34]. We tested 30 different initial surface configurations and all the relaxed structures showed a buckled surface geometry, where half of the surface Si atoms (21/42 atoms) bond with the underlying Si layer. Among the other half Si atoms with dangling bonds, several Si atoms exhibit an  $sp^2$  hybridization with nearly flat geometry, while the others are buckled up (HB-Si) with an average buckling height around 1.1 Å (1.088–1.142 Å) showing an  $sp^3$  hybridization with electron lone pair (see Fig. S6 [34]). This indicates charge transfer from the nearly flat to the HB-Si atoms [34]. As listed in Table SI [34], most of the structures have eight or nine HB-Si atoms, except for two structures that contain seven and ten HB-Si atoms, corresponding to an HB-Si site density (HSD) of 8/21, 9/21, 7/21, and 10/21, respectively [34]. As shown in Fig. 4(a), the structure with seven HB-Si atoms is actually a “local” BHS surface. More importantly, the HB-Si atoms of all the structures show mainly two patterns, as demonstrated by hexagons and ribbons in Fig. S7 [34], indicating the existence of either hexagonally or linearly arranged  $\pi$  conjugations formed by the  $p_z$  orbitals of unbuckled Si atoms (Fig. 4). This further confirms the  $\pi$ -conjugation plus charge-transfer

mechanism in the compressively strained Si(111) surface is general.

The structure with linear  $\pi$  conjugation was found to have the lowest energy with an HSD of 9/21 [Fig. 4(c)]. We noticed that this linearly conjugated pattern is similar to the buckling model (BM) proposed for the  $(2 \times 1)$  surface reconstruction with an HSD of 1/2 [Fig. 4(d)] [44], so we also calculated the surface energy of the BM. Although the BM surface has almost the same unstrained surface energy as the BHS surface, it is easily relaxed to the more stable Pandy  $\pi$ -bonded chain structure due to its similar strong anisotropic stress feature. Interestingly, a highly symmetric  $(\sqrt{21} \times \sqrt{21})$  superstructure with isotropic stress was discovered with an HSD of 9/21 [Fig. 4(b)], which highly resembles a recently experimentally observed structure in the Si(111) surface [35]. Besides the

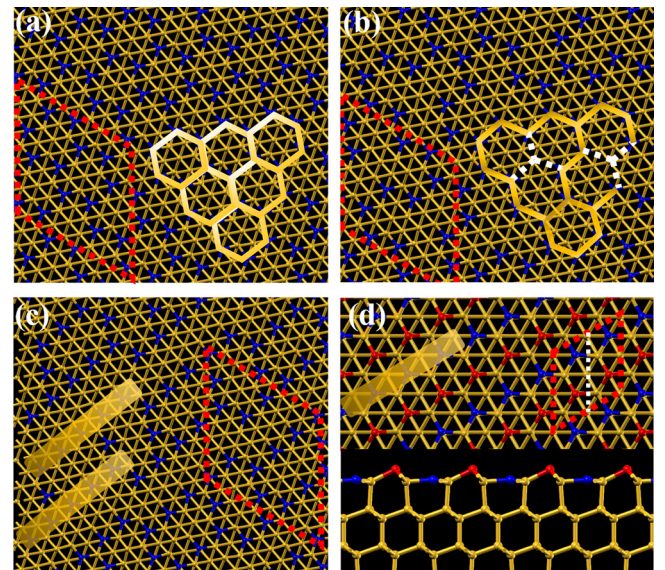


FIG. 4.  $\pi$ -conjugation and charge-transfer model in the  $(\sqrt{21} \times \sqrt{21})$  unit cell, as indicated by the red dashed rhombus. (a) Reproduced  $(\sqrt{3} \times \sqrt{3})$  surface reconstruction with  $\pi$  conjugation formed by the unbuckled Si atoms (blue atoms), as indicated by yellow superhexagons. (b) Metastable highly symmetric  $(\sqrt{21} \times \sqrt{21})$  surface reconstruction. The white dashed lines indicate the breaking of  $(\sqrt{3} \times \sqrt{3})$  hexagonal  $\pi$  conjugation. (c) Linear  $\pi$ -conjugation surface reconstruction as indicated by yellow ribbons. (d) Ideal buckling model for the  $(2 \times 1)$  surface reconstruction.

seven HB-Si atoms that form the  $(\sqrt{3} \times \sqrt{3})$  triangular lattice, two more Si atoms sitting at the center of the two green triangles are slightly buckled up (see Fig. S6 [34]). The buckling of these two atoms partially breaks the  $(\sqrt{3} \times \sqrt{3})$  hexagonal  $\pi$  conjugation [dashed white lines in Fig. 4(b)], which increases slightly the energy by 0.03 eV of the whole system compared to the “local” BHS surface. The surface energies as a function of strain were also calculated to be  $\gamma_{(\sqrt{21} \times \sqrt{21})}(\varepsilon) = 91.1 + 136.1\varepsilon$  (meV/ $\text{\AA}^2$ ), which is very close to the BHS surface, indicating a high structural stability under compressive strain.

In conclusion, we have revealed a cooperative mechanism of hexagonal ring-shaped  $\pi$  conjugation and charge transfer, which stabilizes the recently observed epitaxial Si(111)- $(\sqrt{3} \times \sqrt{3})$  surface with a bamboo hat bonding geometry. It differs dramatically from the commonly known bonding struc-

tures in Si surfaces. It is found to be metastable compared to the bulk-terminated Si(111)-(2  $\times$  1) surface under compressive strain, consistent with the experiments [16–18]. Moreover, as observed in experiments, the  $(\sqrt{3} \times \sqrt{3})$  structure we proposed can form without an Ag overlayer, is persistent over different Si layer thicknesses, and exhibits a linear band dispersion. These findings broaden our knowledge of reconstruction mechanisms on Si surfaces, which also shed light on understanding the difficulties of growing monolayer silicene. It may also have important implications in other epitaxial semiconductor films when grown on strained substrates.

W.J. was supported by the NSF-MRSEC (Grant No. DMR-1121252). X.N. and F.L. acknowledge additional support from U.S. DOE-BES (Grant No. DE-FG02-04ER46148). We thank the CHPC at the University of Utah and DOE-NERSC for providing the computing resources.

- 
- [1] A. W. Hofmann, *Proc. R. Soc. Lond.* **8**, 1 (1856).
  - [2] G. Schultz, *Eur. J. Inorg. Chem.* **23**, 1265 (1890).
  - [3] A. J. Rocke, *Angew. Chem., Int. Ed. Engl.* **54**, 46 (2015).
  - [4] P. Debye and P. Scherrer, *Physik. Z.* **17**, 277 (1916).
  - [5] J. D. Bernal, *Proc. R. Soc. London* **106**, 749 (1924).
  - [6] R. M. Feenstra, W. A. Thompson, and A. P. Fein, *Phys. Rev. Lett.* **56**, 608 (1986).
  - [7] F. J. Himpsel, P. Heimann, and D. E. Eastman, *Phys. Rev. B* **24**, 2003 (1981).
  - [8] K. C. Pandey, *Phys. Rev. Lett.* **47**, 1913 (1981).
  - [9] E. F. Sheka, *Int. J. Quantum Chem.* **113**, 612 (2013).
  - [10] S. Cahangirov, M. Topsakal, E. Aktürk, H. Sahin, and S. Ciraci, *Phys. Rev. Lett.* **102**, 236804 (2009).
  - [11] P. Vogt, P. D. Padova, C. Quaresima, J. Avila, E. Frantzeskakis, M. C. Asensio, A. Resta, B. Ealet, and G. L. Lay, *Phys. Rev. Lett.* **108**, 155501 (2012).
  - [12] L. Chen, H. Li, B. Feng, Z. Ding, J. Qiu, P. Cheng, K. Wu, and S. Meng, *Phys. Rev. Lett.* **110**, 085504 (2013).
  - [13] L. Meng, Y. Wang, L. Zhang, S. Du, R. Wu, L. Li, Y. Zhang, G. Li, H. Zhou, W. A. Hofer, and H. J. Gao, *Nano Lett.* **13**, 685 (2013).
  - [14] L. Tao, E. Cinquanta, D. Chiappe, C. Grazianetti, M. Fanciulli, M. Dubey, A. Molle, and D. Akinwande, *Nat. Nanotechnol.* **10**, 227 (2015).
  - [15] P. D. Padova, P. Vogt, A. Resta, J. Avila, I. Razado-Colambo, C. Quaresima, C. Ottaviani, B. Olivieri, T. Bruhn, T. Hirahara, T. Shirai, S. Hasegawa, M. C. Asensio, and G. L. Lay, *Appl. Phys. Lett.* **102**, 163106 (2013).
  - [16] J. Chen, Y. Du, Z. Li, W. Li, B. Feng, J. Qiu, P. Cheng, S. X. Dou, L. Chen, and K. Wu, *Sci. Rep.* **5**, 13590 (2015).
  - [17] P. D. Padova, A. Generosi, B. Paci, C. Ottaviani, C. Quaresima, B. Olivieri, E. Salomon, T. Angot, and G. L. Lay, *2D Mater.* **3**, 031011 (2016).
  - [18] L. Chen, C.-C. Liu, B. Feng, X. He, P. Cheng, Z. Ding, S. Meng, Y. Yao, and K. Wu, *Phys. Rev. Lett.* **109**, 056804 (2012).
  - [19] H. Fu, L. Chen, J. Chen, J. Qiu, Z. Ding, J. Zhang, K. Wu, H. Li, and S. Meng, *Nanoscale* **7**, 15880 (2015).
  - [20] Z. X. Guo and A. Oshiyama, *New J. Phys.* **17**, 045028 (2015).
  - [21] P. D. Padova, J. Avila, A. Resta, I. Razado-Colambo, C. Quaresima, C. Ottaviani, B. Olivieri, T. Bruhn, P. Vogt, M. C. Asensio, and G. L. Lay, *J. Phys.: Condens. Matter* **25**, 382202 (2013).
  - [22] F. Liu, M. Hohage, and M. G. Lagally, in *Structure of Surfaces and Interfaces, Encyclopedia of Applied Physics, Supplemental Volume*, edited by H. Immergut and G. Trigg (Wiley-VCH, London, 1999), pp. 321–352.
  - [23] G. H. Lu, M. H. Huang, M. Cuma, and F. Liu, *Surf. Sci.* **588**, 61 (2005).
  - [24] F. K. Men, F. Liu, P. J. Wang, C. H. Chen, D. L. Cheng, J. L. Lin, and F. J. Himpel, *Phys. Rev. Lett.* **88**, 096105 (2002).
  - [25] N. Matsumoto, *Jpn. J. Appl. Phys.* **37**, 5425 (1998).
  - [26] F. A. Zwanenburg, A. S. Dzurak, A. Morello, M. Y. Simmons, L. C. L. Hollenberg, G. Klimeck, S. Rogge, S. N. Coppersmith, and M. A. Eriksson, *Rev. Mod. Phys.* **85**, 961 (2013).
  - [27] H. N. Waltenburg and J. T. Yates, Jr., *Chem. Rev.* **95**, 1589 (1995).
  - [28] G. Binnig, H. Rohrer, C. Gerber, and E. Weibel, *Phys. Rev. Lett.* **50**, 120 (1983).
  - [29] D. J. Chadi, *Phys. Rev. Lett.* **43**, 43 (1979).
  - [30] M. Zhou, W. Ming, Z. Liu, Z. F. Wang, P. Li, and F. Liu, *Proc. Natl. Acad. Sci. USA* **111**, 14378 (2014).
  - [31] Z. F. Wang and F. Liu, *Phys. Rev. Lett.* **115**, 026803 (2015).
  - [32] M. Zhou, W. Ming, Z. Liu, Z. F. Wang, Y. G. Yao, and F. Liu, *Sci. Rep.* **4**, 7102 (2014).
  - [33] B. Huang, K. H. Jin, H. L. Zhuang, L. Zhang, and F. Liu, *Phys. Rev. B* **93**, 115117 (2016).
  - [34] See Supplemental Material at <http://link.aps.org/supplemental/10.1103/PhysRevB.95.241405> for discussions on calculation methods, BHS monolayer structure model analysis, tight-binding and Wannier simulations, surface stress tensor, and Si(111)- $(\sqrt{21} \times \sqrt{21})$  surface reconstruction calculations.
  - [35] Z. Li *et al.* (private communication).
  - [36] P. Pflugradt, L. Matthes, and F. Bechstedt, *Phys. Rev. B* **89**, 035403 (2014).

- [37] C. B. Duke, *Chem. Rev.* **96**, 1237 (1996).
- [38] G. A. Somorjai, *Chem. Rev.* **96**, 1223 (1996).
- [39] F. Liu, F. Wu, and M. G. Lagally, *Chem. Rev.* **97**, 1045 (1997).
- [40] V. O. Özçelik and S. Ciraci, *J. Phys. Chem. C* **117**, 26305 (2013).
- [41] V. O. Özçelik, E. Durgun, and S. Ciraci, *J. Phys. Chem. Lett.* **5**, 2694 (2014).
- [42] S. Cahangirov, V. O. Özçelik, A. Rubio, and S. Ciraci, *Phys. Rev. B* **90**, 085426 (2014).
- [43] R. J. Jaccodine, *J. Electrochem. Soc.* **110**, 524 (1963).
- [44] D. Haneman, *Phys. Rev.* **121**, 1093 (1961).